International Journal of Mechanical and Production Engineering Research and Development (IJMPERD)
ISSN (P): 2249–6890; ISSN (E): 2249–8001
Vol. 11, Issue 6, Dec 2021, 237–256

Original Article

DESIGN, CONSTRUCTION AND TESTING OF A LOW-SPEED WIND TUNNEL

KUMARESAN CUNDEN & PROFESSOR FREDDIE L. INAMBAO

School of Mechanical Engineering, University of KwaZulu-Natal, Durban, South Africa

ABSTRACT

The increase in wind energy over the last decade has depicted a significant development in onshore and offshore wind turbine designs. Wind turbine designs are highly dependent on aerodynamic properties of lift and drag. There is normally an iterative process consisting of numerical design, prototype construction, testing and optimisation, calibration of computational flow models on the path to commercialisation. Theoretical turbine models are usually validated or optimised by the assessment of scaled models tested in a wind tunnel. The aim of this paper was to design and manufacture a small-scale low-speed wind tunnel for the testing and optimisation of novel wind turbines. An open circuit design was chosen instead of a closed system to save space. The wind tunnel was to achieve maximum flow speeds of 9m/s in alignment to average wind speeds located off the South African coastline as investigated in previous studies. The conditions within the testing area of the design were required to maintain steady flow conditions. A hot wire wind anemometer was used to measure the flow speeds at different points of the wind tunnel for the validation of the design. The results showed that each section of the wind tunnel complied to the design conditions with minimum error. The turbulence intensity was also investigated and depicted across the circuit. The results have shown that the design philosophy which was chosen was sound and the system may be pursued for the testing of novel scaled wind turbines and scaled aerodynamic profiles for validation and optimisation purposes.

KEYWORDS: South Africa, Wind Tunnel & Offshore Wind Turbines

Received: Aug 24, 2021; **Accepted**: Sep 14, 2021; **Published**: Nov 06, 2021; **Paper Id.**: IJMPERDDEC202115

1. INTRODUCTION

The current versions of wind tunnels have been in existence for roughly 150 years. Prior to this, the best approach was to attach a scaled model to a whirling arm as first utilised by Benjamin Robins (1707 – 1751) which made a large contribution to the early study of fluid mechanics [1], [2].

There are many different wind tunnel design types depending on the application. Wind tunnels which are classified based on the velocity of the fluid in the test chamber are known as subsonic, transonic, supersonic and hypersonic [3]. The Mach number can be used as a simplified way of understanding the type of wind tunnel being used. The subsonic wind tunnel (M < 3) can vary in cross-sectional area of the test section from less than 1 m x 1 m to systems large enough to encompass a full scale industrial truck or large aircraft models [4]. The testing of scaled wind tunnel models is tested in subsonic wind tunnels.

There are various aerodynamic phenomena which can occur at low speeds and low Reynolds numbers, one being a laminar separation bubble which may lead to a decrease in lift as well as an increase in drag leading instability, and unintended vibrational response [5]–[8]. Computational models are usually conducted and validated or optimised via wind tunnel testing and such models are used throughout research facilities, universities, governmental organisations and industry [4]. Some studies have been conducted in the past decades

which have proved some of the capabilities of robust mathematical models for simulations of aerofoils at both high and low Reynolds numbers which can be found in [9]–[11].

Wind tunnels are widely used to conduct aerodynamic tests for full or scaled versions of components [12]–[15]. These systems assist engineers to make appropriate design decisions and aid researchers in understanding thermo-fluid systems. Wind tunnels provide an appropriate means for researchers, engineers, and scientists to investigate complex thermo-fluid dynamic problems which are not always adequately captured by computational models and numerical simulations.

This study aimed to design a wind tunnel capable of being used to test a small-scale vertical axis wind turbine which was designed and elaborated in [16]–[18]. An open circuit design was chosen as this type of wind tunnel design has shown reliable results in previous researchers investigations [19], [20]. This research paper consists of the methodology used, the design methods applied, the phased construction of the wind tunnel system, and the results from the system.

2. METHODOLOGY

The wind tunnel was designed and fabricated for the purpose of testing a novel wind turbine airfoil design as described in [16], [18]. The wind tunnel was required to have suitable scaled contraction, with test and diffuser sections being capable of developing a 9 m/s fluid velocity within the testing chamber. This value was based on the average wind speed observed in [21] for potential offshore wind sites. The following methodological factors were applied to design, calibrate and test the wind tunnel system:

- A maximum turbine diameter (Φ) and height of 150 mm
- A maximum target fluid speed of 9 m/s in the testing chamber
- Selection of appropriate axial fan DC fan controller
- Calibration of wind tunnel axial fan
- Calibration of test chamber incremental steps
- Measure flow speeds at each section
- Evaluate the turbulence intensity of each section

3. DESIGN OF WIND TUNNEL

The axial fan was obtained first as the wind tunnel design constraints were dependent on the maximum wind speed of the fan chosen. A market scan was conducted of both DC and AC powered fans. The price was also a factor in choosing an appropriate cost-effective axial fan. A light 12 V DC fan was chosen and sourced from a light vehicle radiator unit. This led to obtaining a 300 mm, 12 V, 80 W radiator fan with a 30 A AC to DC power supply to meet the electrical demand of the fan. A market scan was conducted for various DC motor controllers with a variable potentiometer for controlling the pulse width modulation (PWM) waveform output to the motor by varying the resistance to effectively change the DC voltage supply.

Fluid flow in piping or ducting requires movement of fluid for the desired result of the system being utilised

(i.e., refinery piping, water reticulation networks, power station cooling networks etc.). All these systems experience some form of losses – major and minor. Major losses are normally due to frictional effects in fully developed flow which is dependent on the area of the duct. Minor losses are normally the result of inlets and exits due to area changes in the ducting system [22].

The selected wind tunnel system was split into four major sections, namely, the settling chamber, contraction (inlet), testing (middle) and diffuser (exit) sections with an open circuit wind tunnel design. The first part of the system was responsible for taking air from a natural atmospheric state and developing the flow to achieve laminar conditions via the settling chamber. The contraction nozzle was designed to accelerate the flow to desired speeds with minimum losses and turbulence to the flow entering the testing section of the system. The testing section was required to have a fluid speed of 9m/s to meet the mean wind speed conditions investigated in [21]. The diffuser section of the wind tunnel was designed based on the constraint of the axial fan maximum speed.

3.1 Settling Chamber

The settling chamber has a uniform cross-sectional area over its length [8] as its function was to stabilise the flow entering the system. The settling chamber was designed to achieve laminar conditions within the testing region of the wind tunnel. This is normally done by utilising some form of laminar flow element (LFE) [23] which resembles a group of straws covering the inlet flow area. Each straw element was narrow enough to achieve a Reynolds Number less than R_{crit} ($R_{crit} \approx 2300$) shown in equation (1) below [22].

$$Re^{Crit} = \frac{\rho V_{tube} D_{tube}}{\mu} \quad (1)$$

where: Re_{Crit}- Reynolds number for laminar flow (Crit ≈ 2300); ρ - Fluid density (kg/m^3); V_{tube} - Fluid Velocity (m/s); D_{tube}-Diameter of tube (m); μ - Dynamic viscosity of air (kg/m·s)

The minimum diameter of the tube elements was found to be ≈ 34 mm when setting the Reynolds number to 2300. The straws being used had a diameter of 5 mm resulting in a Reynolds number of 338.39 which was suitable to develop stable flow for the test section of the wind tunnel. The plastic straws, which were grouped in bundles of 55 to 60 individual straws, were utilised as laminar flow elements. is a graphical representation and layout of the planned settling chamber.

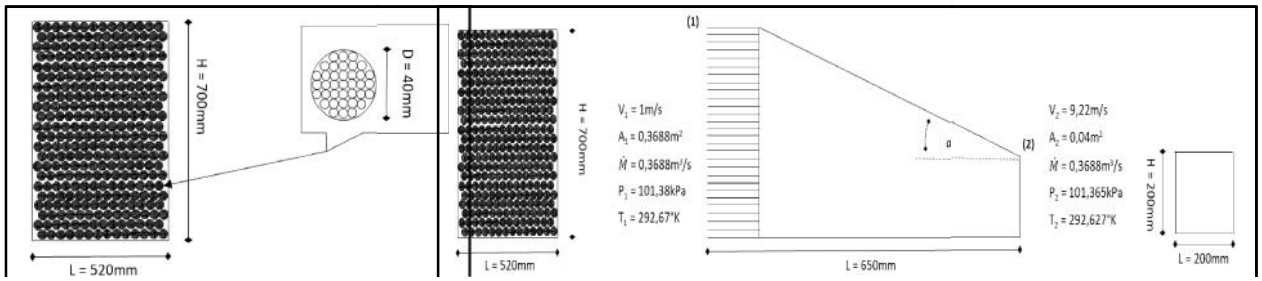

Figure 1: Settling Chamber Figure 2: Settling and Contraction Section.

The straws were stacked vertically, as shown in , so as to cover the entire inlet of the contraction section. By arranging the straws in this way, the incoming flow was segmented into various stream tubes to develop the flow to a

laminar state through a smaller hydraulic area. The flow rate for the entire hydraulic area equates to the sum of the flow rates of each laminar flow element as well as the linear pressure drop relationship to achieve laminar flow [22].

3.2 Contraction Section

The contraction section of the wind tunnel was directly coupled to the settling chamber. The purpose of this section of the wind tunnel was to accelerate the fluid flow to the testing section by gradually reducing the cross-sectional area per a unit distance from the settling chamber. The contraction angle (α) was designed at ≈ 20° from a height of 700mm reducing to 200mm over a length of 500mm.

The fan output was assumed to be 4 m/s based on initial testing of the fan without completion of the full wind tunnel, as the fan induces flow through the system. The mass flow rate was calculated based on the continuity equation (2) [22], [24] and taking the density of air to be constant throughout the system. The mass flow rate was calculated to be 0.3688 m^3/s using an area of 0.09 m^2 for the fan. Using this the inlet and exit velocities of the contraction section were found to be 1 m/s and 9.22 m/s respectively.

$$\dot{M} = \rho V A \quad (2)$$

where:

$\dot{M}$ Mass flow rate (m^3/s)

V Flow velocity (m/s)

A Hydraulic cross section area (m^2)

ρ Flow density (kg/m^3)

For systems where the flow rate is relatively low resulting in subsonic conditions, the fluid behaves as if it is an incompressible fluid. For the purpose of calculating initial gas states at key points of the wind tunnel, it was assumed that the flow was isentropic since the changes in flow variables across the entire system were gradual and not significantly large. The isentropic process allows for changes in the thermodynamic variables of a gas, although the heat capacity of the substance is required to be constant [25]. For this design, the heat capacity of the system was assumed constant resulting in the ratio of specific heats (equation 3) being constant [24].

$$k \equiv \frac{C_p}{C_v} \quad (3)$$

where: k - Ratio of specific heats (-); C_p - Specific heat at constant pressure (); C_v- Specific heat at constant volume ()

To check if the entire wind tunnel can be classified as a subsonic system, a Mach number is needed. If the Mach number is less than 1 the flow regime is classified as subsonic and if the Mach number is greater than 1 the flow regime is classified as supersonic. The Mach number is defined in equation (4) and is the relationship of the fluid velocity to the speed of sound of the same fluid:

$$M = \frac{V}{c} \quad (4)$$

where: M - Mach number (-); V - Fluid velocity (m/s); c - Speed of sound at fluid state (m/s)

Since the fluid is air and is modelled around the ideal gas equation, the speed of sound is a function of specific heats and temperature of the fluid. The speed of sound of the fluid can be calculated with equation (5) to attain the Mach number.

$$c = \sqrt{kRT} \quad (5)$$

where: c - Speed of sound (m/s); k - Ratio of specific heats (-); R - Unique gas constant (-);T - Fluid temperature (°K)

The speed of sound corresponding to the fluid velocity found at the exit of the contraction section was 343.11 m/s at a temperature of 20 °C. The Mach number for the test section was calculated to be 0.027 which was significantly lower than 1, classifying the wind tunnel system as a subsonic system. As stated above, for subsonic conditions the flow regime may be treated as incompressible flow throughout the system, taking heat capacities as constant [22], [24], [25]. The Bernoulli equation (6) is commonly used to determine the static pressure of the system by understanding the dynamic pressure via the velocities as calculated above and illustrated in **Error! Reference source not found.**. This was reduced to equation (7) taking that the static head differential between all points of the system is 0 m as the system is horizontally orientated.

$$P_1 + \frac{1}{2}\rho V_1^2 + \rho g h_1 = P_2 + \frac{1}{2}\rho V_2^2 + \rho g h_2 \quad (6)$$

$$P_1 + \frac{1}{2}\rho V_1^2 = P_2 + \frac{1}{2}\rho V_2^2 \quad (7)$$

where: P - Pressure (kPa); V- Flow velocity (m/s); ρ- Flow density (kg/m^3); h - Static head (m)

Equation (7) was a suitable method for calculating the pressure of each section of the wind tunnel. However, incorporation of the specific heat capacities of the fluid resulted in more accurate calculations, so stagnation equivalents were used as the enthalpy and internal energy components were also catered for. The stagnation state values are equivalent state variables as if the flow was adiabatically reduced to stationary [24].

$$\frac{T_o}{T_{ref}} = 1 + \frac{\kappa - 1}{2} M_{Ref}^2 \quad (8)$$

$$\frac{\rho_o}{\rho_{ref}} = \left[1 + \frac{\kappa - 1}{2} M_{Ref}^2\right]^{\kappa/(\kappa-1)} \quad (9)$$

$$\frac{P_o}{P_{ref}} = \left[1 + \frac{k-1}{2} M^{Ref^2}\right]^{k/(k-1)} \quad (10)$$

where: T_o, ρ_o,P_o - Stagnation state variables (temperature – K, density – kg/m^3, pressure – Pa); T, ρ, P_o

Temperature – K, density – kg/m^3, pressure – Pa; M - Mach number (-); k - Ratio of specific heats (-)

The surrounding ambient thermodynamic air state was used as initial reference gas properties which was applied to equations (8) to (10). Taking the reference gas state conditions shown at the inlet of the contraction section in **Error! Reference source not found.** above, the Mach number was 0.003, and the stagnation pressure (P_o) and stagnation temperature (T_o) were 101.38 kPa and 292.67 °K, respectively. These values were used to compute the outlet pressure (P_2) of the contraction section and local temperature (T_2) which were found to be 101.365 kPa and 292.627 °K, respectively.

Equation (11) was used as a standard thermodynamic method for determining the change in entropy from the contraction inlet to outlet. The change of entropy was 0.0409 kJ/kg·K which may be an indication of friction in the system not factored in previously.

$$s^2 - s^1 = C^P \ln\frac{T_2}{T_1} - R \ln\frac{P_2}{P_1} \quad (11)$$

where: s_2- s_1 - Change in entropy (kJ/kg·K); C_P - Specific heat at constant pressure (-); T - Fluid temperature (°K); Unique gas constant (-); P Fluid pressure (kPa)

The contraction section is a nozzle which accelerates the fluid flow to the testing chamber and can also be assessed by understanding the relationship between the inlet cross-sectional area to the outlet of the contraction section which is referred to as the nozzle area ratio. This parameter should be large enough to attain maximum fluid acceleration and low total pressure losses in the upstream settling chamber [8]. Studies from [26] indicate that a nozzle contraction ratio which is in the range of 6 to 10 is adequate. Ratios below 6 results in higher pressure losses in the upstream sections typically at the screens used for laminar development, while ratios higher than 10 are not beneficial to the system fluid mechanics and is wasteful. The nozzle ratio of the current system was found to be 9.17 which is in line with the findings of [26].

The values calculated for the settling and contraction sections seemed to have been adequate to achieve the desired results at the test section of the wind tunnel. The states from the output of the contraction section were used as input for the test section of the wind tunnel.

3.3 Test Section

The turbine which was designed in [16], [17] and was further developed and numerically assessed in [18], utilised a Selig S1046 blade profile with the centre of mass at roughly 30 % of the blade profile. The turbine was constrained based on the maximum width of the testing chamber ± 180 mm considering clearance and tolerances for the turbine in the section. **Error! Reference source not found.** illustrates the testing chamber for the turbine, where the turbine was located on axis (a).

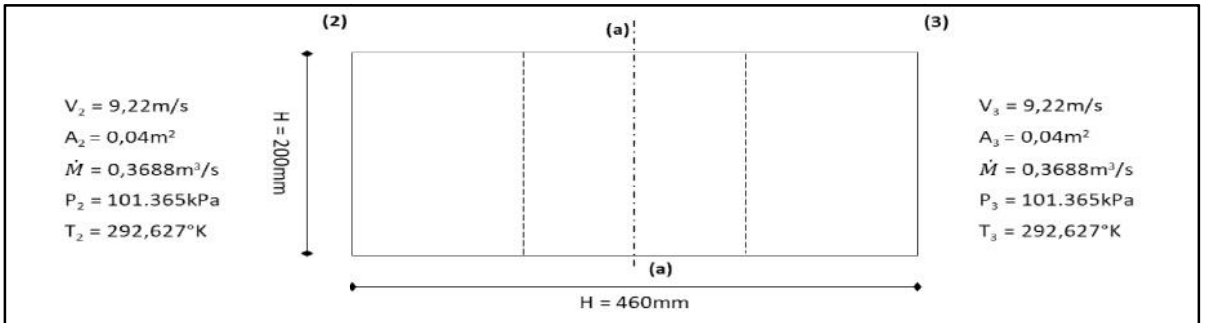

Figure 3: Testing Section.

The test section of the wind tunnel was designed to encompass one turbine to test torque and potential output power from the design in an effort to validate designs presented in [18] which was an adaptation from the designs of [16]. The testing section was assumed to be frictionless for the design phase to have negligible pressure drop over the length of the section.

Findings which were reported in [27] indicate that the testing chamber length would be best suited in a range of 0.5 to 3 times that of the inlet cross-sectional area. This was because of the flow requiring a minimum of 0.5 times that of the cross-sectional area to develop the flow from the contraction section and avoid boundary layer separation. If lengths of the test section exceed 3 times the length of the inlet cross-sectional area, boundary thickness may occur. The test section which was designed had a length which was 2.3 times that of the hydraulic inlet area, which was acceptable.

3.4 Diffuser Section

Since the chosen wind tunnel system was based on an open circuit design the position of the fan was chosen to be located at the end of the diffuser to have an induced fluid flow field. This allowed the fluid to be pulled through the system passing through the settling chamber for flow straightening, entering the contraction section for accelerating the flow to the test section and finally recovering the flow via the diffuser and out the system from the work done by the axial fan.

Within the diffuser section of the wind tunnel there is a relationship between the cross-sectional area of the fan to that of the testing section outlet area or inlet of the diffuser. As shown in [26] an aspect ratio range is imposed on the relationship between the fan and testing outlet cross-sectional areas which is shown in equation (12):

$$2 \leq \frac{A_{Fan}}{A_{Test\ Section}} \leq 3 \quad (12)$$

where: $A_{\_Fan}$ - Cross-sectional area of Fan (m^2); $A_{(\text{Test Section})}$ Cross-sectional area of test section (m^2)

The aspect ratio of the diffuser section was found to be 2.83 which was adequate as ratios above 3 results in irregular fan inlet flow speeds and lower than 2 causes an increase in wind tunnel dimension and fabrication costs. **Error! Reference source not found.** shows the fluid flow states from the inlet to the outlet of the diffuser and through the axial fan. The thermodynamic states were achieved by using equations (8) to (10) with reference values because of the testing chamber analysis.

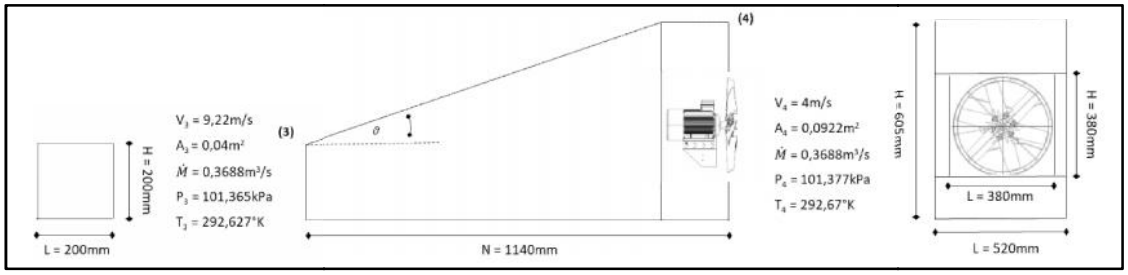

Figure 4: Diffuser Section.

A 12 V DC radiator fan was sourced (80 W) for the system which can generate a flow velocity of 4 m/s to 5 m/s. However, the fan required an appropriate controller to control the flow speed whilst testing the turbine over fluid velocities from 0 m/s to 9 m/s in increments of 0.5 m/s steps of analysis. The hydraulic area of the fan was 0.0962 m^2 utilising a hydraulic radius of 350 mm. The diverging angle of the diffuser (θ) was found to be 18.43° from the horizontal over a length of 1,14 m. The state equation (10) was used to find the outlet diffuser pressure, shown above, which shows suitable recovery through the diffuser section.

4. CONSTRUCTION

This section shows the construction of the wind tunnel system. Simple materials were used based on ease of supply and affordable prices. Each section of the wind tunnel was constructed separately and then joined via the section bases.

Table 1: Materials List – Settling Chamber and Contraction Section

Section	Materials	Size (L x B x W)	Qnt.
Settling chamber	Pine wood	700 mm x 22 mm x 22 mm	2
	Pine wood	520 mm x 22 mm x 22 mm	2
	Masonite	80 mm x 520 mm x 3 mm	1
	Steel straight bracket	45 mm x 45 mm x 15 mm	8
	Steel L bracket	40 mm x 15 mm x 3 mm	4
	Wood screw	3.5 mm x 16 mm	19
	Mesh	3.5 mm x 16 mm	1
	Plastic straws	530 mm x 720 mm	± 15,000
Contraction section	Pine wood	5 mm x 100 mm	2
	Pine wood	700 mm x 22 mm x 22 mm	2
	Pine wood	520 mm x 22 mm x 22 mm	2
	Pine wood	460 mm x 22 mm x 22 mm	1
	Pine wood	230 mm x 22 mm x 22 mm	4
	Masonite	650 mm x 22 mm x 22 mm	2
	Masonite	500 mm x 520 mm x 3 mm	1
	Wood screw	3.5 mm x 16 mm	10

The materials used for the construction were pine wood, Masonite, wood screws, masking tape, rubber sealer and glue. The exterior aesthetic of the system did not affect the performance of the wind tunnel, so this was not considered as a priority in the design. The construction of the wind tunnel also catered for key testing points in the system for the testing of wind speed and temperature.

Error! Reference source not found. shows the material list for the construction of the settling chamber and contraction section. The mesh served as an extra layer of hydraulic refinement after the laminar flow elements and as a screen to hold the bundles of straw in place as flow was induced through the system.

Error! Reference source not found. shows the front and top view of the settling (a) and combined settling and contraction section (b) of the wind tunnel. The points highlighted in (b) as (1) and (2) are testing sections which corresponds to **Error! Reference source not found.**. Test holes were drilled with a diameter of 20 mm to allow for the anemometer used for measuring wind velocity.

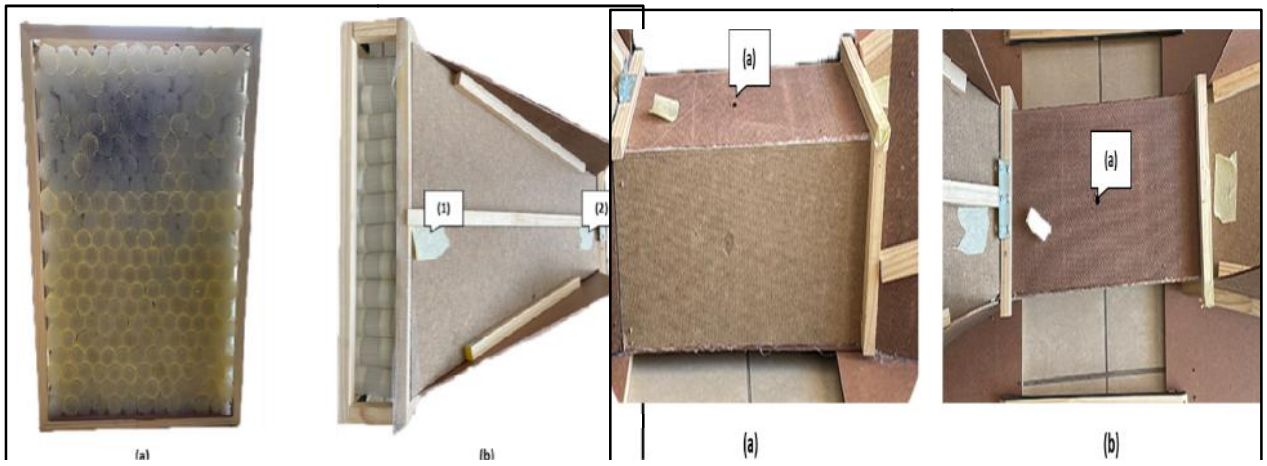

Figure 5: Constructed Settling Chamber and Contraction Section – Figure 6: Testing Section – (a) Side View, (b) Top View (a) Front View of Settling Chamber, (b) Top View of Settling and Contraction Section.

The materials used for this section of the wind tunnel was Masonite board as shown above and rubber seal which was used to ensure minimum leakage. Masonite was chosen for each of the sections due to the smooth profile of one side reducing friction losses in the system. **Error! Reference source not found.** shows the material list for the testing section of the tunnel.

Table 2: Materials List – Testing Section

Section	Materials	Size (L x B x W)	Qnt.
Testing Section	Masonite	460mm x 210mm x 3mm	4
	Rubber seal	840mm x 15mm x 3mm	2

Error! Reference source not found. shows the constructed testing section of the tunnel where the turbine would be subjected to aerodynamic loading. **Error! Reference source not found.** (a) depicts the side view and (b) the top view of the section of the system. The point indicated (a) in both pictures corresponds to the axis shown in **Error! Reference source not found.** above.

Error! Reference source not found. shows the top view (a), side view (b) and the front view of the fan (c). The points labelled (3) and (4) correspond to the points indicated in **Error! Reference source not found.** above. The materials list for the diffuser section and fan section are reflected in **Error! Reference source not found.**.

Table 3: Materials List – Diffuser and Fan Section

Section	Materials	Size (L x B x W)	Qnt.
Diffuser section	Pine wood	850 mm x 22 mm x 22 mm	2
	Pine wood	700 mm x 22 mm x 22 mm	2
	Masonite	1000 mm x 650 mm x 3 mm	2
	Masonite	1000 mm x 520 mm x 3 mm	1
	Steel straight bracket	45 mm x 45 mm x 15 mm	2
	Steel L bracket	40 mm x 15 mm x 3 mm	4
	Wood screw	3.5 mm x 16 mm	30
Fan section	Pine wood	700 mm x 22 mm x 90 mm	2
	Pine wood	500 mm x 22 mm x 90 mm	2
	Pine wood	650 mm x 22 mm x 22 mm	1
	Pine wood	230 mm x 22 mm x 22 mm	4
	Masonite	1000 mm x 500 mm x 3 mm	1
	Masonite	650 mm x 500 mm x 3 mm	2

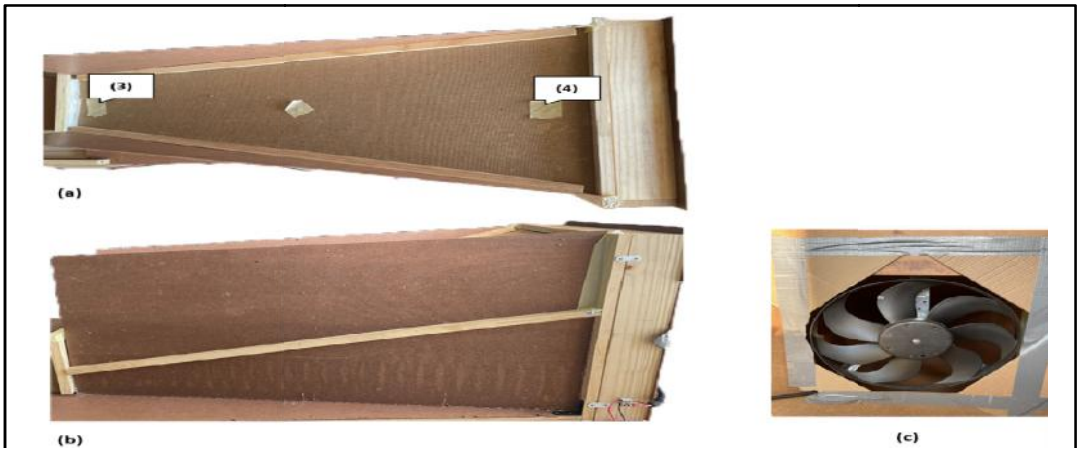

Figure 7: Diffuser Section and Fan – (a) Diffuser Top View, (b) Diffuser Side View, (c) Fan.

The system was joined together via the base of each section of the tunnel. The fan required DC power for operation so a 12 V AC to DC power supply was sourced (**Error! Reference source not found.**). The fan was set to operate on constant full load rating if connected to the power supply directly. To control the fluid flow within the test section, proper control of the fan was required.

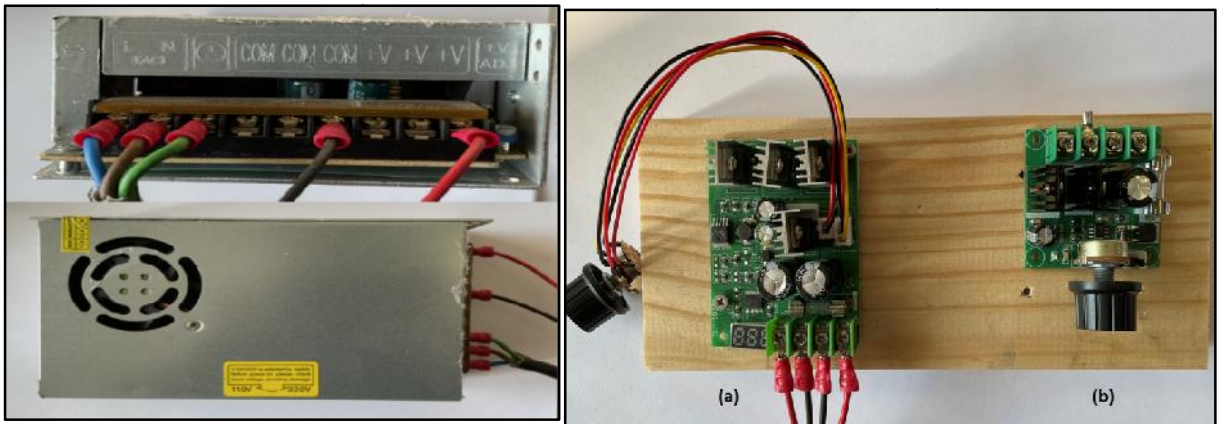

Figure 8: AC to DC Power Supply Figure 9: Motor Controllers – (a) 30 A, (b) 8 A.

Currently motor controllers are pulse width modulation (PWM) controllers. By adjusting the potentiometer on

the device, the duty cycle of the motor is changed resulting in speed control via controlling the voltage. Initially an 8 A PWM controller was sourced but on testing it was not sufficient to control the motor stably at full load. This led to obtaining a larger 30 A PWM motor controller which ran the fan at full load without any fluctuations in output as experienced by the 8 A motor controller. Both motor controllers are shown in **Error! Reference source not found.**.

Error! Reference source not found. (a) shows the controller which was chosen which has a linear relationship with the DC output voltage in relation to the percentage output of the LED when using the potentiometer to control the PWM output. This led to the mapping of the fan speed to the testing section speed which will be elaborated upon in the next section.

5. CONTROL AND INSTRUMENTATION

The following section of the paper explains the different tools and devices used for the control and instrumentation of the system to measure suitable variables in the wind tunnel. The major instruments which were used was a wind anemometer for flow speed and temperature and the motor controller for induced flow control. The methodology applied was to map the controller percentage output, reflected on the LCD shown in **Error! Reference source not found.** (a), with the test section speed in increments of 0.5 m/s.

A portable handheld sensor was used for measuring flow speed so as not as to cause major disturbances to the flow. A hot wire anemometer was chosen. This device also had telescopic capability which resulted in ease of measurement at the extremities of the contraction and diffuser inlet and out sections respectively. **Error! Reference source not found.** shows the anemometer which was used to measure the flow and temperature of the system. The devices' data was logged in per second readings in comma separated value format (.csv) which was exported and analysed in Microsoft Excel. However statistical data cleaning was required to the logged data which is further explained in the results section of the article.

Sensor type	**Hot wire**
Measuring range	0 to 6,000 fpm
Accuracy	±(20 fpm +5 % of m.v.) (0 to 394 fpm) ±(59 fpm +5 % of m.v.) (394 to +3,000 fpm)
Resolution	1.97 fpm
Volume flow (cfm)	0 to 99,999 cfm (Resolution: 0.1 cfm)
Sensor type	**NTC**
Measuring range	-4 to 140 °F
Accuracy	±0.9 °F
Resolution	0.1 °F
General technical data	
Compatibility	requires iOS 8.3 (or later) / Android 4.3 (or later) requires mobile device with Bluetooth 4.0
Storage temperature	-4 to 140 °F
Operating temperature	-4 to 122 °F
Battery type	3 AAA Batteries (incl.)
Battery life	15 hrs
Dimensions	7.9 x 1.2 x 1.6 in Telescope extendable to 15.7 in.
Warranty	2 years
Measuring Units	°F, °C, fpm, m/s, cfm, m³/h, l/s

Figure 10: Hot Wire Wind Anemometer.

As shown in **Error! Reference source not found.**, a motor control was used to control the fan speed. The motor controller chosen also had a linear relationship with the output DC voltage being regulated by the potentiometer to control the motor. **Error! Reference source not found.** shows the mapping of the controller output to the 0.5 m/s

increments for flow speed in the testing chamber of the wind tunnel system.

Table 4: Mapping of DC Controller to Test Section Flow Speed

Percentage	Voltage [DC]
0%	0,00
5%	0,58
10%	1,15
15%	1,73
20%	2,30
25%	2,88
30%	3,45
35%	4,03
40%	4,60
45%	5,18
50%	5,75
55%	1,00
60%	6,90
65%	7,48
70%	8,05
75%	8,63
80%	9,20
85%	9,78
90%	10,35
95%	10,93
100%	11,50

Test Section Speed	Percentage	Voltage [DC]
0,50	15%	1,73
1,00	19%	2,17
1,50	22%	2,53
2,00	29%	3,34
2,50	33%	3,80
3,00	38%	4,37
3,50	43%	4,95
4,00	48%	5,52
4,50	51%	5,87
5,00	57%	6,56
5,50	61%	7,02
6,00	66%	7,59
6,50	71%	8,17
7,00	76%	8,74
7,50	81%	9,32
8,00	86%	9,89
8,50	91%	10,47
9,00	96%	11,04
9,50	99%	11,39

6. RESULTS AND DISCUSSIONS

This section of the research shows the results from the testing points reflected in Table 4 to validate the design of the wind tunnel system. The data from the anemometer is read as comma separated values and processed in Microsoft Excel. To evaluate the system at various testing points on the wind tunnel, the tests were conducted for a period of 5 minutes resulting in 300 data points for sampling. However, for the incremental changes and calibrating the fan, the testing period was 1 minute per increment with a settling time of 45 seconds. The wind tunnel results were taken from testing the system at full load conditions as the assumption was the conditions below full load would be valid based on the results from full loading of the fan.

There were five key testing points on the wind tunnel which started at the entrance of the contraction section (outlet of the settling chamber) towards the exit of the contraction chamber then onto the testing section and followed by the diffuser inlet and diffuser exit readings. The average flow speed, the stagnation pressure and the turbulence intensity were investigated from the data gathered. The researchers in [28] utilised the root mean square (RMS) method to post process the measured hot wire anemometer data to understand the turbulence intensity. The turbulence intensity is defined in equation (13) as the ratio of velocity fluctuations from the mean freestream velocity [8], [29], [30].

$$T.I. = \frac{u'_{RMS}}{U_\infty} \quad (13)$$

where: *T.I.* Turbulence intensity (%); u'_{RMS} - Root mean square of the velocity fluctuations (m/s); U_∞ Mean

flow velocity (m/s)

The RMS is normally used when the distribution is known and typically Gaussian in shape, however, the distribution of the sample set was not known in this instance. Researchers in [31] demonstrated that the standard RMS formula should be corrected with the variance being considered and applied. The term u'_{RMS} was defined as the amount of velocity fluctuation from the mean velocity for the measured sample in the total population size. After applying this correction, the turbulence intensities were resolved as per equation (13) above.

The turbulence intensity at each point of measurement in the system was calculated based on empirical readings as this is an input parameter in the computation fluid dynamic (CFD) model within the two turbulence transport equations being k-ε and k-ω respectively. The *k* term of the transport equation defines the turbulent kinetic energy and the *ε* term represents the dissipation of the turbulent energy. The ω term can be taken as the specific turbulence dissipation and is the rate at which the fluid is converted into internal thermal energy [32]. Equation (14) shows the relationship between *k* and turbulence intensity.

$$k = \frac{3}{2}(IU)^2 \quad (14)$$

where: *k* - Turbulent kinetic energy (J/kg); *I* - Turbulence intensity (%); *U* - Mean flow velocity (m/s)

6.1 Settling Chamber

Pre- and post-construction of the settling section measurements were conducted at the test chamber of the system to gauge the flow regime with and without a settling chamber. The measurement was based on incremental changes to the fan speed resulting in roughly 0.5 m/s velocity intervals for a 30 second duration. The following results show the change in stability of the flow shown in **Error! Reference source not found.**.

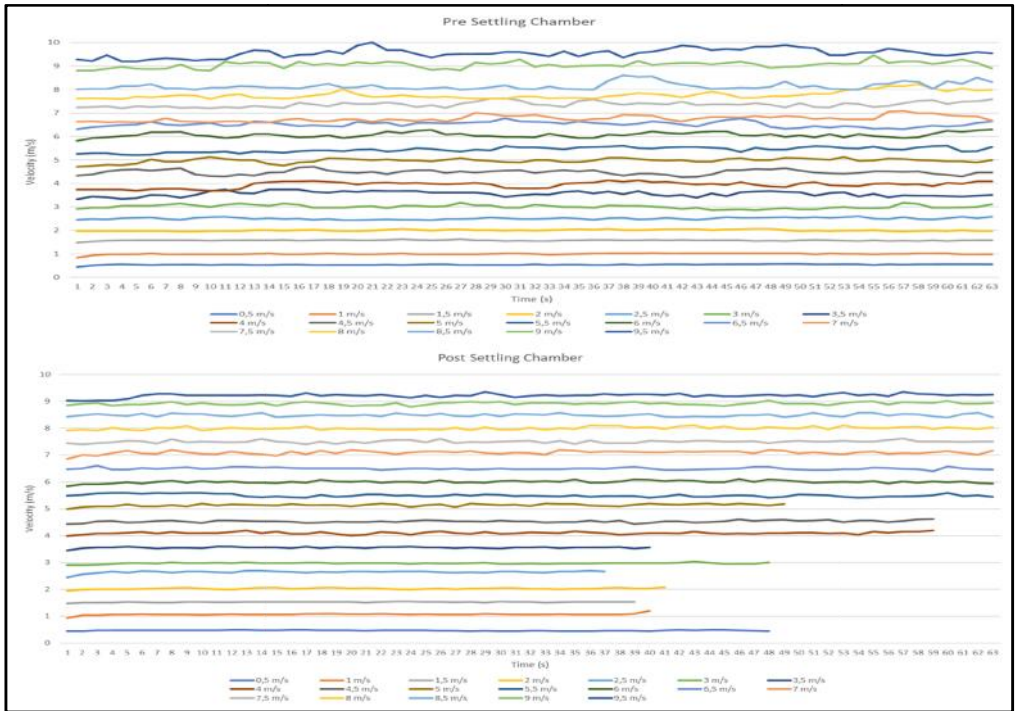

Figure 11: Pre-Settling and Post-Settling Chamber Results.

Error! Reference source not found. also depicts the results after the addition of the settling chamber laminar flow elements. There was a significant change in the stability of the flow after testing section speeds increased passed 3 m/s. The introduction of the laminar flow elements proved the settling chamber flow straightening capabilities at the testing section, demonstrating adequate testing conditions when varying flow speed range incrementally. There are signs of instability over speeds of 7 m/s, however, the disturbance did not significantly affect the testing conditions.

From the settling chamber the fluid enters the contraction section of the system for flow acceleration. During the accelerating process of the flow the fluid experiences minor changes in flow uniformity due to friction and seam joins between sections. **Error! Reference source not found.** shows the results of the instantaneous velocity and turbulence intensity for the inlet of the contraction nozzle. The inlet of the contraction chamber was located at point (A) as shown in **Error! Reference source not found.** and was taken as the resultant output of the settling chamber. The results show a stable velocity profile at full load of the system which is what was required. The averaged state velocity, temperature, Mach number and pressure were found to be 1.096 m/s, 292.67 °K, 0.00319 kPa and 101.38 kPa respectively. The turbulence intensity was calculated to be 0.84 % for the section showing that the settling chamber had successfully developed the flow to a laminar state.

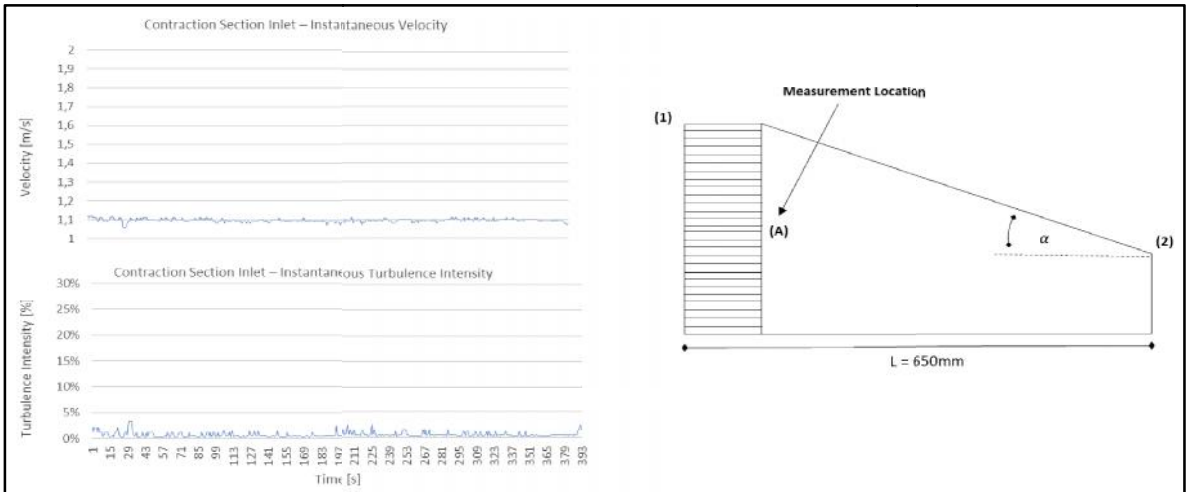

Figure 12: Contraction Nozzle Inlet – Velocity and Turbulence Intensity.

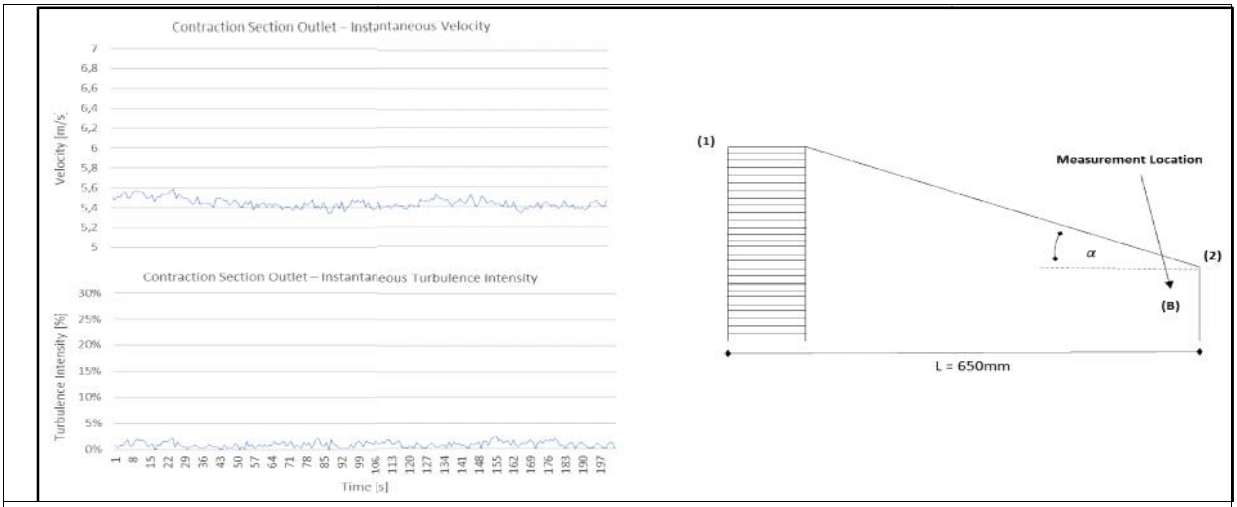

Figure 13: Contraction Nozzle Outlet – Velocity and Turbulence Intensity.

Error! Reference source not found. shows the results from the measurements taken at point (B) shown in the figure for the outlet of the contraction nozzle. The average accelerated flow velocity at (B) was found to be 5.44 m/s, an increase of 4.9 x that of the inlet speed of 1.096 m/s. The averaged state variables were 5.44 m/s, 293.25 °K, Mach number of 0.016 and 101.37 kPa taken as inlet conditions for the test section of the system. The turbulence intensity was 0.98 %.

The testing section results are shown in **Error! Reference source not found.** below which were measured at point (C). As stated in [27] the flow requires a minimum of 0.5 times the hydraulic diameter or length for the flow to fully develop from the contraction nozzle outlet. This was taken into consideration and the test results were recorded at a distance equivalent to the hydraulic length (200 mm) from the outlet of the contraction section. This measurement location was also taken to be adequate for the testing of the turbine as proposed in [16]–[18] for future experiments.

The results shown in **Error! Reference source not found.** show that the fluid accelerated adequately to meet the desired fluid velocity of 9 m/s with the section reaching an average speed of 9.23 m/s with a turbulence intensity of 0.76 %. This proved that the testing section had adequate stable developed flow for the testing of turbine designs. The

average temperature within the section was measured to be 292.59 °K, 101.38 kPa and the Mach number was calculated to be 0.0269 and operated at subsonic conditions.

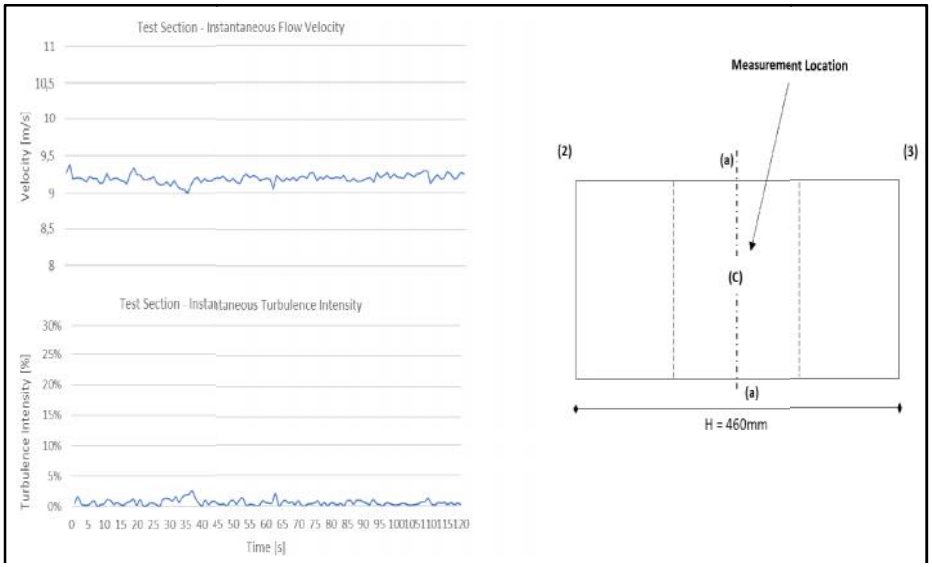

Figure 14: Testing Section – Velocity and Turbulence Intensity.

The diffuser inlet receives fluid flow from the test section was required to recover appropriately before merging back to atmospheric conditions of the large control volume. The results of the inlet sampling points are shown in **Error! Reference source not found.** measured at point (D). It can be seen from the results that the instantaneous velocity measured at the diffuser inlet of the system transitions into an unstable profile in comparison to the previous sections of the system. The averaged state variables for the measured locations for fluid velocity, temperature, Mach number and pressure were 7.67 m/s, 294.18 °K, Mach number of 0.022 and a pressure of 101.28 kPa. The turbulence intensity at this point was calculated to be 0.76 % which was stable and regarded as non-turbulent with a non-steady velocity profile.

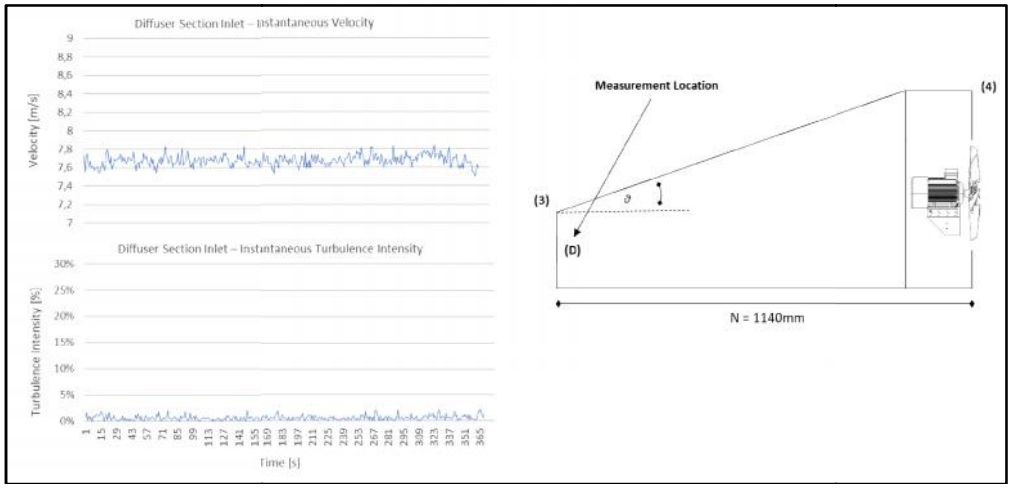

Figure 15: Diffuser Section Inlet – Velocity and Turbulence Intensity.

Error! Reference source not found. shows the results which were obtained from measurements at point (E) of the diffuser section. The instantaneous velocity profile was found to be unstable as this was relatively close to the axial

fan. The state variables for this location were 3.81 m/s mean velocity, fluid temperature of 294.03 °K, a Mach number of 0.011 and pressure of 101.378 kPa. The turbulence intensity for the region was calculated to be 7.91 % which was roughly 9 x higher than the previous sections of the wind tunnel system.

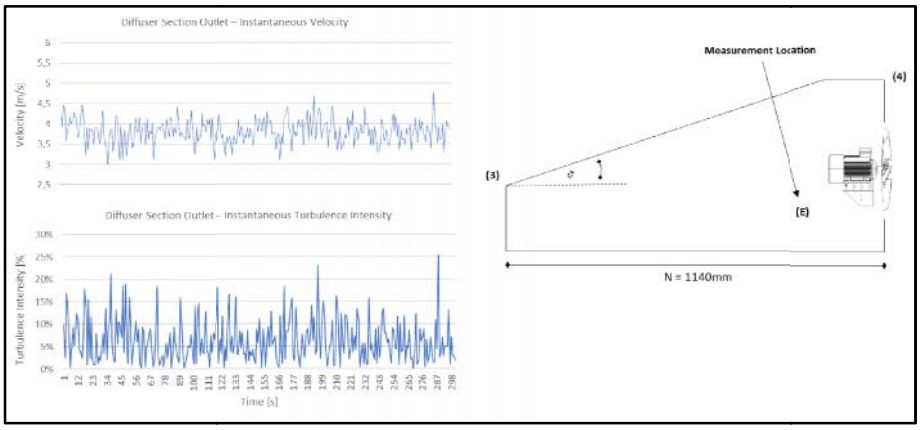

Figure 16: Diffuser Section Outlet – Velocity and Turbulence Intensity.

Error! Reference source not found. shows the aggregated state variable results for all the sampling points identified above in **Error! Reference source not found.**, **Error! Reference source not found.** and **Error! Reference source not found.** respectively. Analysing the results, the state variables are in good agreement with the design requirements as stated above which proves that the wind tunnel system would be suitable to perform tests on the chosen wind turbine.

Table 5: Results from Sampling Points

	[1]	[2]	[3]	[4]	[5]
Mean Velocity [m/s]	1,09	5,44	9,24	7,67	3,81
Stagnation Pressure [kPa]	101,379	101,375	101,365	101,37	101,38
Average Temperature [°K]	292,67	293,25	292,6	294,17	294,03
Mach No.	0,032	0,01585	0,02693	0,02232	0,01109
Turbulence Intensity [%]	0,84	0,98	0,76	0,76	7,91

Table 6: Turbulence Classification

Turbulence	Turbulence Intensity
Very Low	0,05 % - 1 %
Medium	1 % - 5 %
High	5 % - 20 %

Error! Reference source not found. also shows the turbulence intensity of each of the sampling points. It was evident that the laminar flow elements accomplished the desired function of flow straightening from the contraction chamber to the point of entering the diffuser section of the wind tunnel. The high turbulence intensity experienced at point (E) was attributed to the flow fully recovering to atmospheric conditions as well as the influence of the induced draft from the fan. **Error! Reference source not found.** shows the turbulence classification as a function of turbulence intensity [33].

Using this as a benchmark it can be seen that the turbulence profile was very low from the outlet of the settling chamber to the inlet of the diffuser section of the system. These conditions were shown to be in good relation to those of the numerical calculated state variables which proves that this wind tunnel design can be utilised for the testing of novel wind turbines and aerofoils for validation and optimisation.

7. CONCLUSIONS

The research conducted in the study aimed to investigate the design of a low-speed wind tunnel for the purpose of

testing novel wind turbines and aerofoil designs. The system was designed in accordance with best practice from industry in the fields of thermodynamics and fluid dynamics. The wind tunnel was split into four major sections for design purposes, being the settling chamber, the contraction nozzle, the testing section and the diffuser section. Each section was designed and fabricated individually and assembled as a complete system for testing.

The testing of the system was conducted at various points through the operational length of the wind tunnel and measurements were recorded for evaluation and validation of state variables. It was found that the state variables at each measurement location were in good correlation to those of the numerical methods used for the design, thus proving that the design and fabricated wind tunnel was adequate for the testing of wind turbines and aerofoils elaborated in [18], [21].

8. FUTURE WORK

The current system design is planned to be utilised to calculate the potential of the turbine which was designed in [17], [18]. The addition of a microcontroller to simulate meteorological measured conditions is being investigated to understand the turbine's response and electrical output to fluctuating wind loading.

REFERENCES

1. *D. D. Baals and W. R. Corliss, Wind Tunnels of NASA, 1st ed. Washington D.C: Scientific and Technical Information Branch, National Aeronautics and Space Administration, 1981.*
2. *J. D. Jaramillo, "Design and construction of a low speed wind tunnel," Houghton College, 2017.*
3. *T. H. Yong and S. S. Dol, "Design and development of low-cost wind tunnel for educational purpose," 2015, doi: 0.1088/1757-899X/78/1/012039.*
4. *L. Cattafesta, C. Bahr, and J. Mathew, "Fundamentals of wind-tunnel design," Encyclopedia of Aerospace Engineering. John Wiley & Sons, 2010, doi: 10.1002/9780470686652.eae532.*
5. *R. Ricci and S. A. Montelpare, "Quantitative IR thermographic method to study the laminar separation bubble phenomenon," Int. J. Therm. Sci., vol. 44, pp. 709–719, 2005, doi: 10.1016/j.ijthermalsci.2005.02.013.*
6. *R. Ricci, S. A. Montelpare, and E. Silvi, "Study of acoustic disturbances effect on laminar separation bubble by IR thermography," Exp. Therm. Fluid Sci., vol. 31, pp. 349–359, 2007, doi: 10.1016/j.expthermflusci.2005.08.007.*
7. *W. Zhang, R. Hain, and C. J. Kahler, "Scanning PIV investigation of the laminar separation bubble on a SD7003 airfoil," Exp. Fluids, vol. 45, pp. 725–743, 2008, doi: 10.1007/s00348-008-0563-8.*
8. *S. Mauro, S. Brusca, R. Lanzafame, F. Famoso, A. Galvagno, and M. Messina, "Small-scale open-circuit wind tunnel: Design criteria, construction and calibration," Int. J. Appl. Eng. Res., vol. 12, no. 23, pp. 13649–13662, 2017.*
9. *C. P. Mellen, J. Frohlich, and W. Rodi, "Lessons from lesfoil project on large-eddy simulation of flow around an airfoil," AIAA J., vol. 41, pp. 573–581, 2003, doi: 10.2514/2.2005.*
10. *L. Davidson, LESFOIL: Large eddy simulation of flow around a high lift airfoil: Results of the project LESFOIL supported by the European Union 1998-2001. 2003.*
11. *A. Uranga, P. O. Persson, M. Drela, and J. Peraire, "Implicit large eddy simulation of transitional flows over airfoils and wings.," 19th AIAA Computational Fluid Dynamics, 22-25 June, San Antonio, Texas, USA, 2009.*
12. *J. M. Rainbird, J. Peiró, and J. M. R. Graham, "Blockage-tolerant wind tunnel measurements for a NACA 0012 at high*

angles of attack," J. Wind Eng. Ind. Aerodyn., vol. 145, pp. 209–218, 2015, doi: 10.1016/j.jweia.2015.06.006.

13. *H. Sarlak, T. Nishino, J. N. Sørensen, Simos T., and C. Tsitouras, "Urans simulations of separated flow with stall cells over an nrel s826 airfoil," in AIP Conference, 2016, pp. 30–39, doi: 10.1063/1.4951795.*
14. *B. Celis and H. H. Ubbens, "Design and construction of an open-circuit wind tunnel with specific measurement equipment for cycling," Procedia Eng., vol. 147, pp. 98–103, 2016, doi: 10.1016/j.proeng.2016.06.196.*
15. *I. Bayati, M. Belloli, L. Bernini, and A. Zasso, "Aerodynamic design methodology for wind tunnel tests of wind turbine rotors," J. Wind Eng. Ind. Aerodyn., vol. 167, pp. 217–227, 2017, doi: 0.1016/j.jweia.2017.05.004.*
16. *F. L. Inambao and K. Cunden, "Design and numerical simulation of a small scale helical cross flow turbine," in 13th BIE Biennial Conference, 2013, pp. 23–32.*
17. *K. Cunden, "Design of a novel hydrokinetic turbine for ocean current power generation," Master's dissertation, University of KwaZulu-Natal, 2015.*
18. *F. L. Inambao and K. Cunden, "Offshore vertical axis wind turbine simulation," Int. J. Mech. Prod. Eng. Res. Dev., vol. 11, no. 2, pp. 187–204, 2021.*
19. *J. Rajadas and B. Rogers, "Design, fabrication and testing of a low-speed wind tunnel laboratory," ASEE Annu. Conf. Expo. Conf. Proc., 2007, doi: 10.18260/1-2--2150.*
20. *N. Kumar Maurya, M. Maurya, A. Tyagi, and S. P. Dwivedi, "Design & Fabrication of low speed wind tunnel and flow analysis," Int. J. Eng. Technol., no. December, pp. 381–387, 2018, [Online]. Available: https://www.researchgate.net/publication/329872818.*
21. *F. L. Inambao and K. Cunden, "Offshore wind resource assessment off the South African coastline," Int. J. Mech. Eng. Technol., vol. 10, no. 6, pp. 95-119, 2019.*
22. *R. Fox W., P. Pritchard J., and A. McDonald T., "Internal incompressible viscous flow," in Introduction to Fluid Mechanics, John Wiley & Sons, 2009, pp. 328–337.*
23. *G. Millar H, "Laminar flow element and flow meter," US3349619A, 1967.*
24. *R. Fox W., P. Pritchard J., and A. McDonald T., "Introduction to compressible flow," in Introduction to fluid mechanics, John Wiley & Sons, 2009, pp. 582–604.*
25. *National Aeronautics and Space Administration (NASA), "Calorically perfect gas," Isentropic Flow. https://www.grc.nasa.gov/www/BGH/isentrop.html (accessed Apr. 15, 2021).*
26. *J. H. Bell and R. D. Mehta, "Contraction design for small low-speed wind tunnels," 1988. doi: 19890004382.*
27. *J. B. Barlow, W. H. Rae, and A. Pope, Low speed wind tunnel testing, 3rd ed. New York: Wiley-Interscience, 1999.*
28. *K. Pascioni, . Reger, A. Edstrand, and L. Cattafesta, "Characterization of an aeroacoustic wind tunnel facility," INTERNOISE, 43rd International Congress on on Noise Control Engineering: Improving the World through Noise Control, 2014.*
29. *M. Itoh and M. Kobayashi, "Turbulent structure in the three-dimensional boundary layer on a swept wing," in 4th International Symposium on Engineering Turbulence Modelling and Measurements, 1999, pp. 699–708, doi: https://doi.org/10.1016/B978-008043328-8/50067-9.*
30. *A. F. Molland and S. R. Turnock, "6 - Theoretical and numerical methods," in Marine Rudders and Control Surfaces, A. F. Molland and S. R. B. T.-M. R. and C. S. Turnock, Eds. Oxford: Butterworth-Heinemann, 2007, pp. 233–311.*

31. *T. Chai and R. R. Draxler, "Root mean square error (RMSE) or mean absolute error (MAE)?," Geosci. Model Dev., vol. 7, pp. 1525–1534, 2014, doi: 10.5194/gmdd-7-1525-2014.*

32. *D. Apsley, "Computational hydraulics - lecture notes." University of Manchester, 2021, [Online]. Available: https://personalpages.manchester.ac.uk/staff/david.d.apsley/lectures/comphydr/turbmodel.pdf.*

33. *F. Jouse, "Defining turbulent boundary conditions," SimScale CAE Forum, 2016. https://www.simscale.com/forum/t/defining-turbulent-boundary-conditions/80895 (accessed Apr. 10, 2021).*

34. *Pittala, Suresh, and T. Diriba. "Computational Fluid Dynamics Analysis of Impeller Design For A Pump." International Journal of Mechanical Engineering (IJME) 5.4.*

35. *Alrobaian, Abdulrahman A., et al. "A new approach to low-cost open-typed subsonic compressible flow wind tunnel for academic purpose." International Journal of Mechanical and Production 8.6 (2018): 383-394.*

36. *Govardhan, D., and B. Praveen. "Design and Analysis of Two Throat Wind TunneL." International Journal of Mechanical and Production Engineering Research and Development (IJMPERD) 8. 1, Feb 2018, 513 520.*

37. *Prasad, U. Shiva, et al. "Design and analysis of two throat wind tunnel." International Journal of Mechanical and Production Engineering Research and Development 7.4 (2017): 381-388.*